Chaos, Solitons and Fractals 114 (2018) 164–174

Contents lists available at ScienceDirect

Chaos, Solitons and Fractals

Nonlinear Science, and Nonequilibrium and Complex Phenomena

journal homepage: www.elsevier.com/locate/chaos

Impact of hybrid neural network on the early diagnosis of diabetic retinopathy disease from video-oculography signals

Ceren Kaya[a,*], Okan Erkaymaz[b], Orhan Ayar[c], Mahmut Özer[d]

[a] Department of Biomedical Engineering, Zonguldak Bülent Ecevit University, 67100 Zonguldak, Turkey
[b] Department of Computer Engineering, Zonguldak Bülent Ecevit University, 67100 Zonguldak, Turkey
[c] Department of Ophthalmology, Zonguldak Bülent Ecevit University, 67100 Zonguldak, Turkey
[d] Department of Electrical and Electronics Engineering, Zonguldak Bülent Ecevit University, 67100 Zonguldak, Turkey

ARTICLE INFO

Article history:
Received 11 December 2017
Revised 7 June 2018
Accepted 24 June 2018

Keywords:
Video-oculography
Diabetic retinopathy
Wavelet transform
Hilbert–Huang transform
Artificial neural network
Particle swarm optimization

ABSTRACT

In this study, we introduce two hybrid artificial neural network models with particle swarm optimization algorithm to diagnose diabetic retinopathy based on the Video-Oculography signals. The hybrid models use Discrete Wavelet Transform and Hilbert-Huang Transform separately to extract features from the signals. The classification performance of both models is analyzed comparatively. We show that the model based on Hilbert–Huang Transform exhibits better classification performance than the model based on the Discrete Wavelet Transform.

1. Introduction

Diabetic retinopathy occurs in people with diabetes because of damaging the blood vessels in the retina. Diabetic retinopathy involves early and late stages, which are defined as non-proliferative diabetic retinopathy (NPDR) and proliferative diabetic retinopathy (PDR). In early stages (NPDR), fluid leakage on retina blood vessels is observed. In late stages (PDR), new blood vessels are formed on the retina [1]. Diabetic retinopathy is usually diagnosed clinically. In the advanced stages patients have decreased vision due to the complications of the disease. However, in the early stages the changes in ocular structures are just can be seen during routine ocular examination. Optic coherence tomography (OCT) device can be used to detect macular diseases such as diabetic macular edema, vitreomacular traction and epiretinal membranes. Fundus fluorescein angiography (FFA) can be used to detect retinal vascular changes such as ischemia, microaneurysms, artery or vein occlusion [2]. In this context, early detection is significant to limit the potential of vision loss because different medical tests provide information only when disease complications occur.

The disease stage has been detected with image processing and artificial intelligence methods by using retinal images [3–5]. Priya and Aruna [6] compared probabilistic neural network, bayes classifier and support vector machine techniques to classify diabetic retinopathy by using fundus images. Rajput et al. [7] used k-means clustering algorithm and wavelet transform to extract features from retinal fundus images of patients with diabetic retinopathy. Noronha et al. [8] obtained fundus images features by using discrete wavelet transform and classified them by support vector machine algorithm. Rokade and Manza [9] used k nearest neighbor classification and wavelet transform methods to extract hard exudates in retinal images of patients with diabetic retinopathy. Solkar and Das [10] preferred probabilistic neural network and support vector machine techniques to classify diabetic retinopathy by using blood vessel extraction from retinal images.

During the last several decades, physiological signals of eye such as Electrooculography (EOG), Video-Oculography (VOG) and Electroretinography (ERG) have been widely used by physicians to detect eye disorders. In recent years, VOG has become a popular video-based non-invasive measurement method and provides information about eye movements with high accuracy. This method is commonly used to design hardware for tracking eye movements [11]. Clarke et al. [12] presented an eye tracking system which is based on complementary metal-oxide semiconductor (CMOS) image sensors to recognize the pupil and other eye features. The proposed model has not required complicated image processing algorithm. It generally works well when gaze is

* Corresponding author.
E-mail addresses: ceren.kaya@beun.edu.tr, crnkaya@hotmail.com (C. Kaya).

https://doi.org/10.1016/j.chaos.2018.06.034
0960-0779/

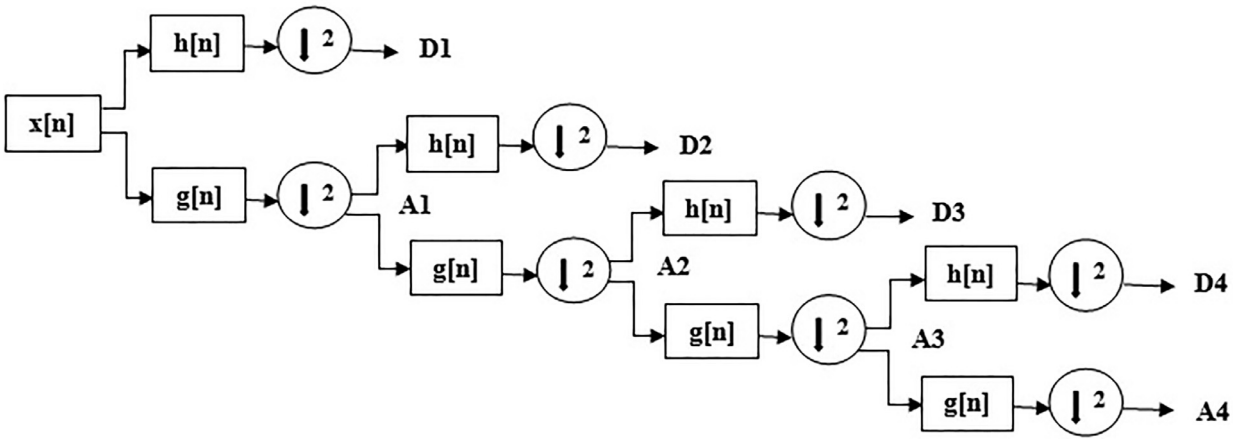

Fig. 1. Signal sub-band decomposition with discrete wavelet transform.

pointing straight ahead, but the system provides large error at eccentric gaze positions. Chen et al. [13] introduced a healthy volunteer to conduct a sinusoidal monitoring test to verify the pupil location for WIFI-based VOG system. They showed that the proposed method performed well. Kim et al. [14] implemented a real-time three-dimensional VOG system which could measure horizontal, vertical and torsional eye movements and calculate the pupil radius. Hanuska et al. [15] reported that patients with Parkinson's disease have longer latencies in vergence eye movements (VEM) metrics obtained by using VOG signals for slower and hypometric divergence. Recently, we proposed multi-layer perceptron and radial basis function neural network models for the classification of diabetic retinopathy disease based on VOG signals [16].

Due to its potential for the diagnosis of diabetic retinopathy, different approaches might be promising to extract crucial information from VOG signals. In this context, different feature extraction methods are required to be applied for the pre-processing phase of VOG signals. Therefore, in this study we propose a new hybrid decision support system to diagnose levels of diabetic retinopathy by using horizontal and vertical VOG signals. The hybrid decision support system, ANNPSO consists of a conventional Artificial Neural Network (ANN) with a training part based on Particle Swarm optimization (PSO). For this aim, we consider both Discrete Wavelet Transform (DWT) and Hilbert-Huang Transform (HHT) to extract statistical features of VOG signals. We comparatively attempt to show the classification performances of DWT-ANNPSO and HHT-ANNPSO models for diagnosis of disease. We also examine the statistical performance of both models based on the confusion matrix.

In our previous study [16], the observed VOG dataset includes 21 samples and three classes (Healthy: 7, NPDR: 7 and PDR: 7). The distribution of three classes in the test dataset (4 samples) is not homogenous. Each sample has five statistical features (maximum, minimum, mean, standard deviation and variance) calculated with DWT. The classification model topology has 25 inputs, one output neuron and one hidden layer with 18 neurons for Multilayer Perceptron (MLP) and Radial Basis Function (RBF) models. We trained the MLP and RBF models with training dataset (80% of dataset) for 200 iterations and tested with 20% of dataset. Our results showed that proposed RBF model results in better classification performance than MLP model.

In this study, the observed VOG dataset includes heterogeneous 50 samples and three classes (Healthy: 17, NPDR: 16 and PDR: 17). The distribution of three classes in the test dataset (10 samples) is homogenous. Four statistical features (maximum, minimum, root mean square and standard deviation) are extracted from each sample by using DWT and HHT. The DWT-ANNPSO model has 20 inputs, one output neuron and one hidden layer with 16 neurons. HHT-ANNPSO model has 4, 8, 12 and 16 input neurons respectively for different intrinsic mode function (IMF) groups. We train the DWT-ANNPSO and HHT-ANNPSO models with training dataset (80% of dataset) and test with 20% of dataset. The training phase is conducted with 200 trials including 1000 epochs for both models. Our results show that proposed HHT-ANNPSO model results in better classification performance than DWT-ANNPSO model.

In sum, comparing the study given in [16], our current study has dataset with large size and uses homogeneous random selection algorithm in preparation of training and test dataset. The selected dataset is suitable for the real time decision making in clinical studies. Using of ANNPSO hybrid model to classify diabetic retinopathy with VOG signal is the novelty in literature. The proposed model is more compact designed with small input and hidden layer size than our previous study.

2. Materials and methods

We propose a new hybrid decision support system to diagnose level of diabetic retinopathy by using horizontal and vertical VOG signals. The system consists of four phases; first phase is the signal measurement, second phase is feature extraction through DWT and HHT methods separately, third phase is classification with proposed hybrid model and fourth phase is optimization of the weights and biases of designed model.

In signal based studies, process of feature extraction is significant in time–frequency domain analysis. Therefore, different signal analysis techniques have been used such as Fourier, Wavelet and Hilbert-Huang transform [17–19]. The wavelet transform is a commonly used method for efficiently signal analysis in time-domain. It exhibits the signals minutiae in the multi-resolution analysis, but wavelet transform can not achieve fine resolutions in both time domain and frequency domain simultaneously [18]. For this reason, HHT has been offered to process non-stationary and nonlinear signals [19]. The HHT is an adaptive signal analysis method that combines the empirical mode decomposition (EMD) and the Hilbert spectral analysis (HSA). Any complicated data set in HHT can be decomposed into a finite and often small number of IMFs [20]. The HHT method which is suitable for analyzing nonlinear and non-stationary data, has been generally used to extract features from

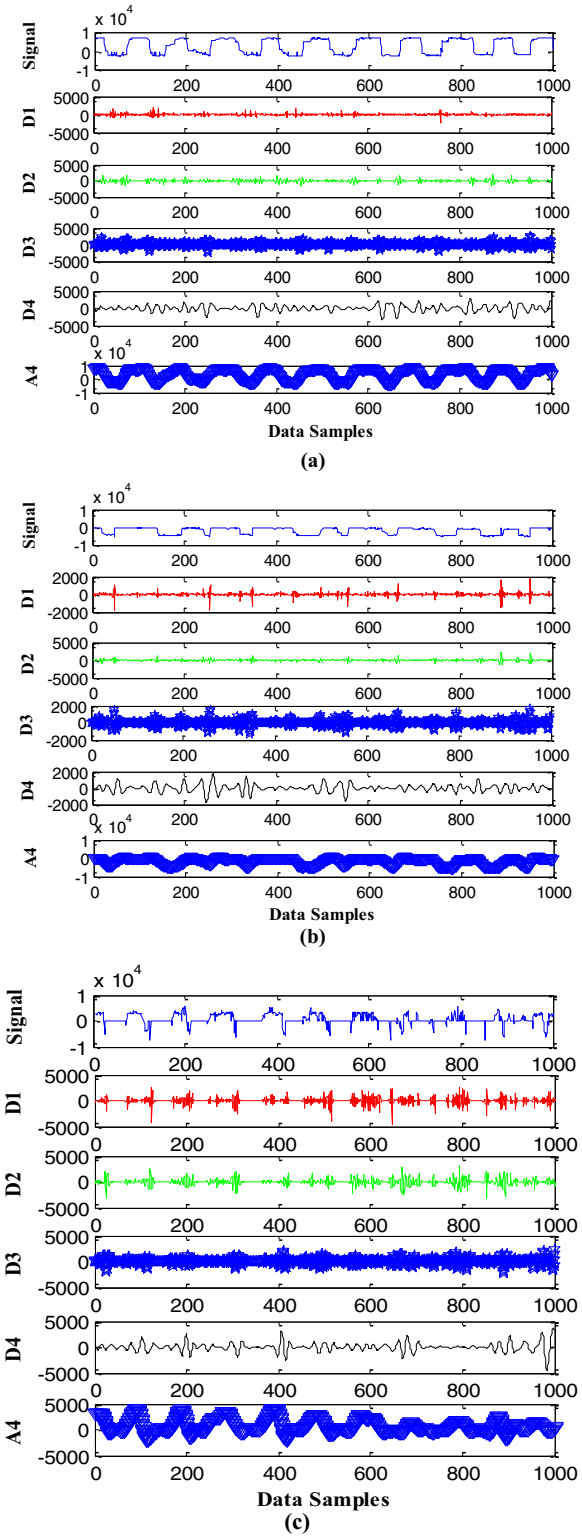

Fig. 2. VOG Signal and its DWT coefficients: a) Healthy, b) NPDR and c) PDR examples.

electrocardiogram (ECG), electromyogram (EMG), skin conductivity (SC) and respiration changes (RSP) [21].

2.1. Dataset

In order to measure accurately the performance of proposed model, a VOG signal dataset is prepared using 200 Hz internal monitoring camera located in the Metrovision MonPackOne Electrooculography device. The observed dataset includes 50 samples and three classes (Healthy: 17, NPDR: 16 and PDR: 17). Four statistical features (maximum, minimum, root mean square and standard deviation) are extracted from each sample by using DWT and HHT.

2.2. Feature extraction

We extract different statistical features with DWT by using 4th level Coiflet wavelet (Coif4) and HHT by decomposing IMFs. The wavelet coefficients are obtained by dividing into sub-band frequencies: approximation (A4) and detail wavelet coefficients (D1-D4) from each VOG signals. Four different statistical features (maximum, minimum, root mean square and standard deviation) are obtained from both wavelet coefficients and HHT IMFs.

2.2.1. DWT

In this study, we first extract statistical features by using DWT. The number of decomposition levels and appropriate wavelet selection are very crucial in DWT method. The wavelet selection depends on the signal to be analyzed. The number of decomposition levels is selected based on the dominant frequency components of the signal [22]. In this study, Coiflet wavelet is used due to its higher scaling capability in signal-processing techniques rather than Haar and Daubechies wavelets [23]. Signal sub-band decomposition with DWT is shown in Fig. 1.

As seen in Fig. 1, the original signal (x[n]) is passed through a high pass filter (g[n]) and a low pass filter (h[n]) to acquire the detail (D1-D2-D3-D4) and approximation (A4) coefficients, respectively. The same operation is continued to determine decomposition level only for approximation coefficients. DWT coefficients of VOG signals, which are taken as feature vectors are calculated by 4th level Coiflet wavelet (Coif4) which leads to a smoother wavelet. The following statistical features (maximum, minimum, root mean square and standard deviation) of the coefficients are calculated for each sub-band to reduce the dimension of feature vectors and represent the time-frequency distribution of VOG signals.

Schneck et al. measured fast oscillation amplitudes of EOG signals obtained from three subject groups (non-diabetic, diabetic without retinopathy and diabetic with retinopathy) and also observed that fast oscillation amplitudes of EOG signals are significantly reduced in both diabetic group compared with healthy group. In addition, they apply statistical ANOVA-Tukey test with $p < 0.01$ significant criteria to show difference between the three subject group measurements. It is shown that there is significant difference among non-diabetic and diabetic group signals ($p < 0.0004$) [24]. In consisted with the results by Schneck et al., we observed that VOG signal amplitudes of the groups with diabetic retinopathy (NPDR and PDR) are less than health group (Fig. 2). Reducing amplitude of VOG signal occurs on change the statistical features of each subject group. We calculated DWT coefficients for each Healthy, NPDR and PDR VOG signals as given in Fig. 2, where high frequency properties (D1-D4) and low frequency properties (A4) during 4th level wavelet decomposition of VOG signal are shown. Amplitude of Healthy VOG signal and its DWT coefficients is higher than NPDR VOG signal and its DWT coefficients. PDR VOG signal and its DWT coefficients have distorted appearance rather than other VOG signal groups.

2.2.2. HHT

We also extract statistical features by using HHT. HHT, which is based on the local characteristics of the signal's time scale and defines the instantaneous frequency, is a time-frequency localization analysis method that is more adaptive than DWT [19].

The HHT consists of two parts: Empirical Mode Decomposition (EMD) and Hilbert Spectral Analysis (HSA). EMD is a key part of the HHT method, where a complex dataset can be decomposed into finite number of IMFs [20]. An IMF is defined as a function that satisfies the following conditions:

(1) In the whole data set, the number of extrema and the number of zero crossings must either equal or differ at most by one.
(2) At any data point, the mean value of the envelope defined using the local maxima and the local minima is zero.

The EMD algorithm is based on a recursive structure called sifting. Given any signal, X(t), the IMFs are computed through the following steps:

a. Initialize i = j = 1.
b. Define all the local extrema of X(t) and divide the extrema into two sets: the maxima and the minima.
c. Then connect all the local maxima by a cubic spine line to form an upper envelope $X_{upper}(t)$. Repeat the procedure for the local minima to form a lower envelope $X_{lower}(t)$.
d. Calculate the mean signal

$$M_{i,j}(t) = \frac{X_{upper}(t) + X_{lower}(t)}{2} \quad (1)$$

e. Subtract the mean $M_{i,j}(t)$ from X(t) to obtain the first candidate to IMF $H_{i,j}(t)$:

$$H_{i,j}(t) = X(t) - M_{i,j}(t) \quad (2)$$

f. Compare conditions of the sifting: If $H_{i,j}(t)$ should satisfy the definition of an IMF, then stop. Else, in the subsequent sifting process, $H_{i,j}(t)$ is treated as the signal for the next round of sifting, and j = j + 1;Then restart the algorithm from Step 2. After repeated sifting, up to k times, if $H_{i,k}(t)$ becomes an IMF, we denote by $c_i(t)$ the first IMF.
g. Set the residue $r_i(t) = X(t) - c_i(t)$ (3); if $r_i(t)$ is less than some predetermined value or becomes non-oscillatory thus the number of IMF's depends on the signal and is not a fixed value, the sifting process can be stopped.

Else, in the subsequent sifting process, $r_i(t)$ is treated as the signal for the next round of sifting, and i = i + 1; then restart the algorithm from Step 2. End when $r_n(t)$ has at most one extrema, after being repeated n times.

By summing up above, we finally obtain:

$$X(t) = \sum_{i=1}^{n} c_i(t) + r_n(t) \quad (4)$$

Thus, the original signal X(t) are decomposed into n IMFs and a residue $r_n(t)$, which can be either the adaptive constant.

In order to provide illustrative examples for the HHT features, we obtained IMFs for Healthy, NPDR and PDR VOG signals by using EMD and plotted respectively, in Figs. 3–5. As seen in Figs. 3 and 4, amplitude of Healthy VOG signal and its four IMFs is higher than NPDR VOG signal and its four IMFs. PDR VOG signal and its four IMFs have disrupted form rather than other VOG signal groups in Fig. 5.

Four statistical features; maximum, minimum, root mean square and standard deviation; are calculated from each IMF after the decomposition of VOG signals by using HHT. These statistical features, used as a single input vector to the ANNPSO classifier, can be seen as a feature extraction step in the diagnosis of diabetic retinopathy.

2.3. ANNPSO classifier

ANN has been widely used in a variety of medical applications because of high generalization capability [25–28]. Therefore, in this study, we use a hybrid ANN model. The model, ANNPSO consists of conventional ANN topology whose training part is based on particle swarm optimization (PSO) algorithm. The model has three layers: an input layer, a hidden layer and an output layer. The statistical features obtained from DWT and HHT methods separately are applied to the input layer. The hidden layer with 16 neurons was created by topology testing.

In the model training phase, we generate the training and test dataset with randomly selected raw dataset that involves three classes (Healthy: 17, NPDR: 16 and PDR: 17 samples). During the selection, the datasets are designed homogeneously to include three classes. The training dataset has 40 samples (80% of the raw dataset) and the test dataset has 10 samples (20% of the raw dataset). Moreover, we perform 200 trials consisting of 1000 epochs for both hybrid models to obtain the best performance. The models use a nature algorithm inspired from the behavior of bird flocks called as a swarm instead of traditional learning algorithms. In this algorithm, each solution is represented as a vector called as a particle (bird) [29]. The population (swarm) may contain any random number of initial particles. Each particle starts with its initial position and velocity, then moves in the solution space to achieve the optimum result [30]. The main computational steps of PSO include generating initial position and velocity of each particle in population and updating position and velocity for a certain number of generations to get the optimal solution [31].

Finally, we determine the classification performance for the models by using accuracy method (confusion matrix). The method expressions are given as follows in Eqs. (5)–(8):

$$\text{Accuracy } (\%) = 100 * \frac{TP + TN}{TP + TN + FP + FN} \quad (5)$$

$$\text{Sensitivity } (\%) = 100 * \frac{TP}{TP + FN} \quad (6)$$

$$\text{Specificity } (\%) = 100 * \frac{TN}{TN + FP} \quad (7)$$

$$\text{False Discovery Rate } (\%) = 100 * \frac{FP}{TP + FP} \quad (8)$$

where FN, FP, TN and TP denote False Negative, False Positive, True Negative and True Positive respectively.

3. Results and discussion

We consider one hybrid classification model for the DWT investigation. The model has 20 inputs, one output neuron and one hidden layer with 16 neurons. We also construct 7 models for HHT investigation. For IMF1,2,3,4; IMF1-2; IMF1-3 and IMF1-4; the models have 4, 8, 12 and 16 input neurons respectively. The weights and biases of the models are optimized by using PSO algorithm. Then, the optimized models are tested with dataset and the performance of the models are observed.

The extracted features of the horizontal VOG signals are shown as an example in Figs. 6–9 for each method (DWT and HHT). Figs. 6 and 7 represent extracted statistical features (maximum, minimum, root mean square and standard deviation) of left and right horizontal DWT coefficients for Healthy, NPDR and PDR VOG signals, where Healthy1, Healthy2, Healthy3, Healthy4 and Healthy5 stands for Healthy VOG signal over D1, D2, D3, D4 and A4 coefficients respectively. The term NPDR is referred to NPDR VOG signal and PDR to PDR VOG signal.

The low-frequency coefficient (A4), which is regarded as the characteristic behavior of the signal, is the most vital component and it includes more information than other wavelet coefficients (D1-D4) [32]. It confirms that the statistical features of obtained DWT coefficients from left and right horizontal VOG signals

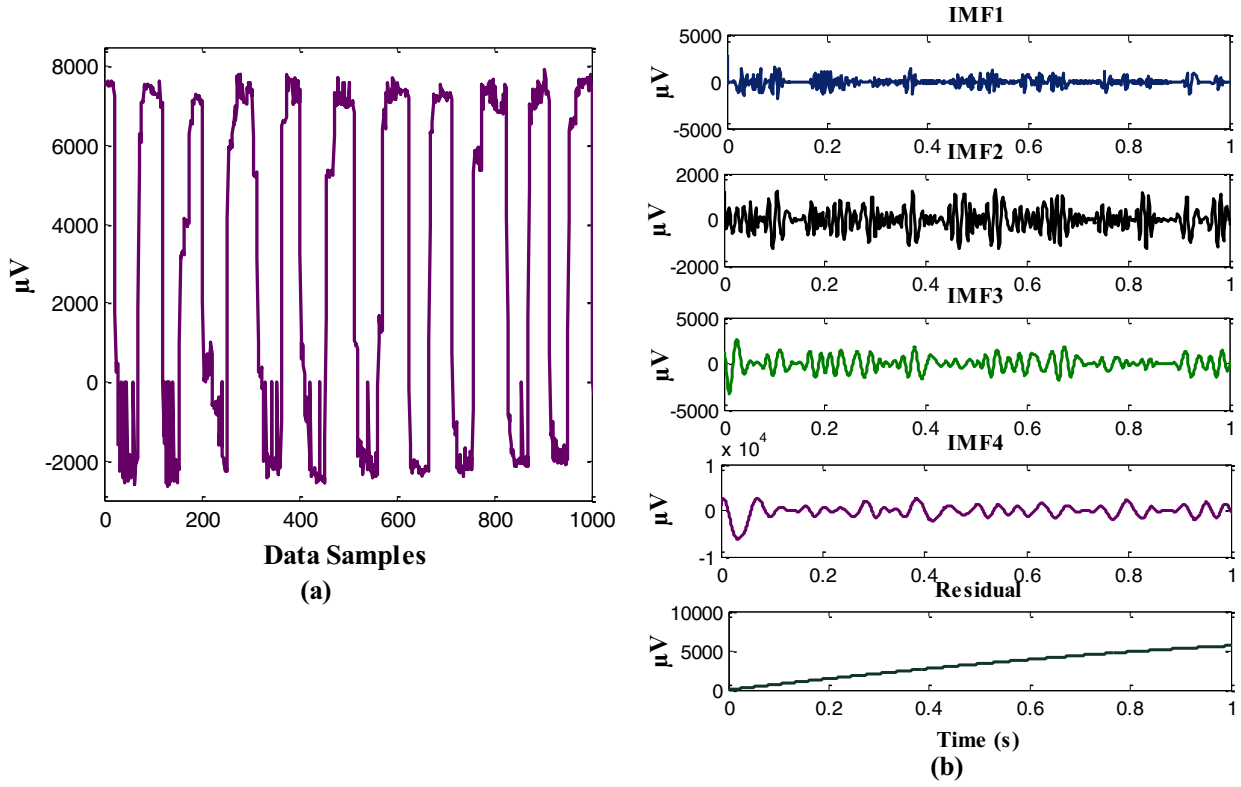

Fig. 3. The components obtained from 4th level EMD decomposition of healthy VOG signal, (a) Healthy VOG signal (Raw Data) (b) Healthy IMFs (IMF1-IMF4) and residual.

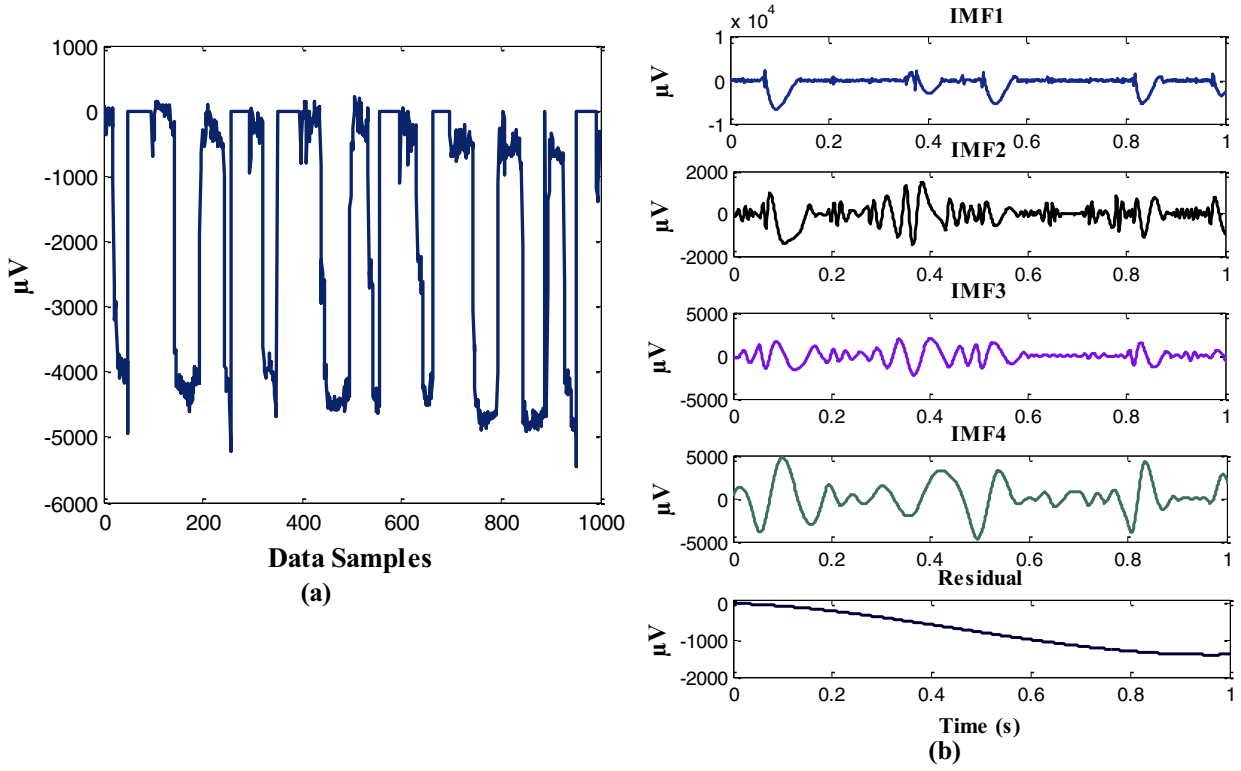

Fig. 4. The components obtained from 4th level EMD decomposition of NPDR VOG signal, (a) NPDR VOG signal (Raw Data) (b) NPDR IMFs (IMF1-IMF4) and residual.

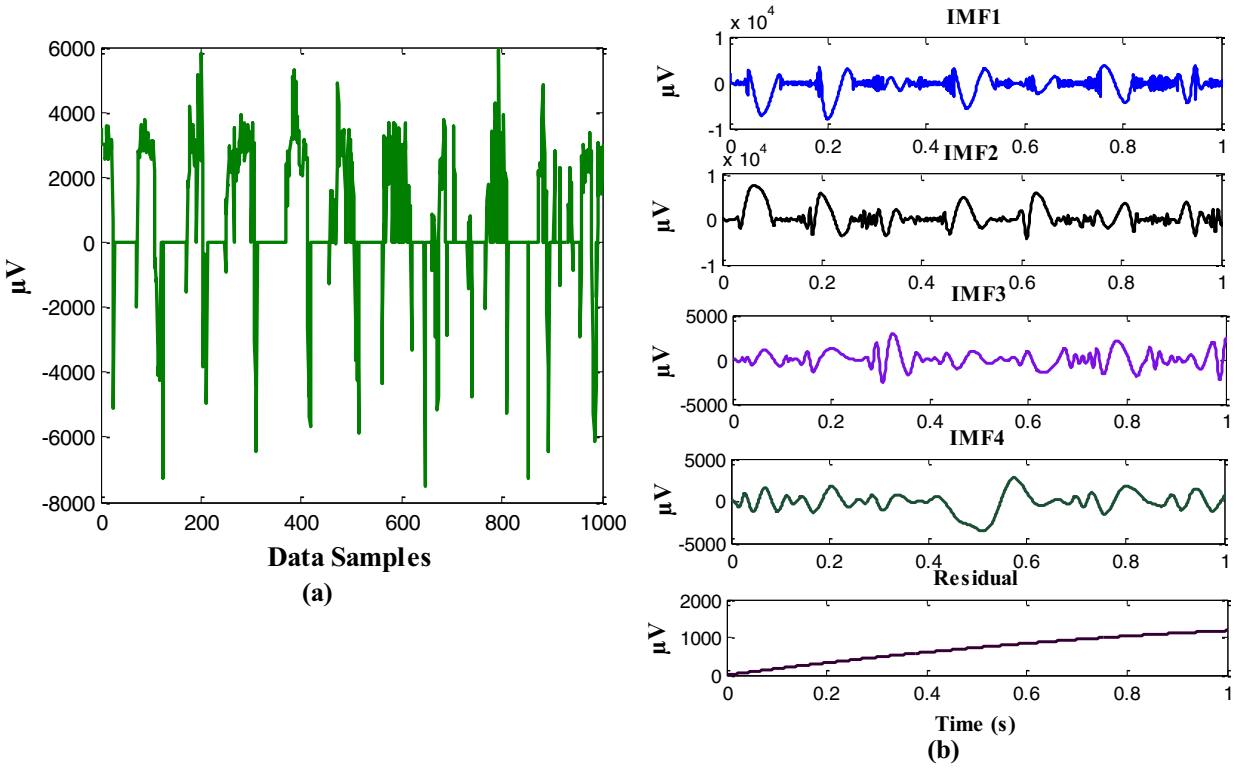

Fig. 5. The components obtained from 4th level EMD decomposition of PDR VOG signal, (a) PDR VOG signal (Raw Data) (b) PDR IMFs (IMF1-IMF4) and residual.

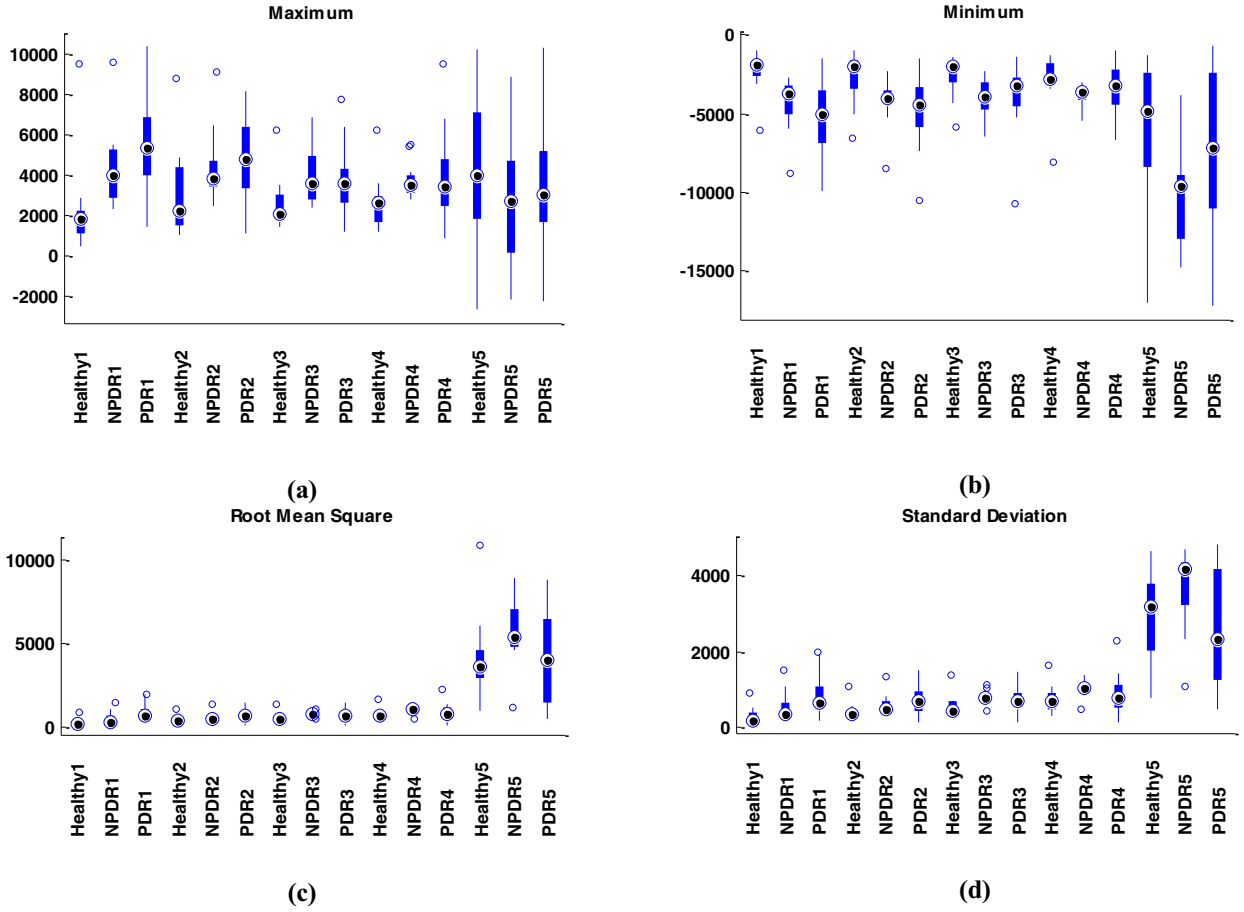

Fig. 6. Statistical features of Left Horizontal DWT coefficients for Healthy, NPDR and PDR VOG Signals (a) maximum, (b) minimum, (c) root mean square and (d) standard deviation. The figure shows range of variation (min-max) and deviations of low-frequency coefficient (A4) and high-frequency coefficients (D1-D4) during wavelet decomposition for left horizontal VOG signal.

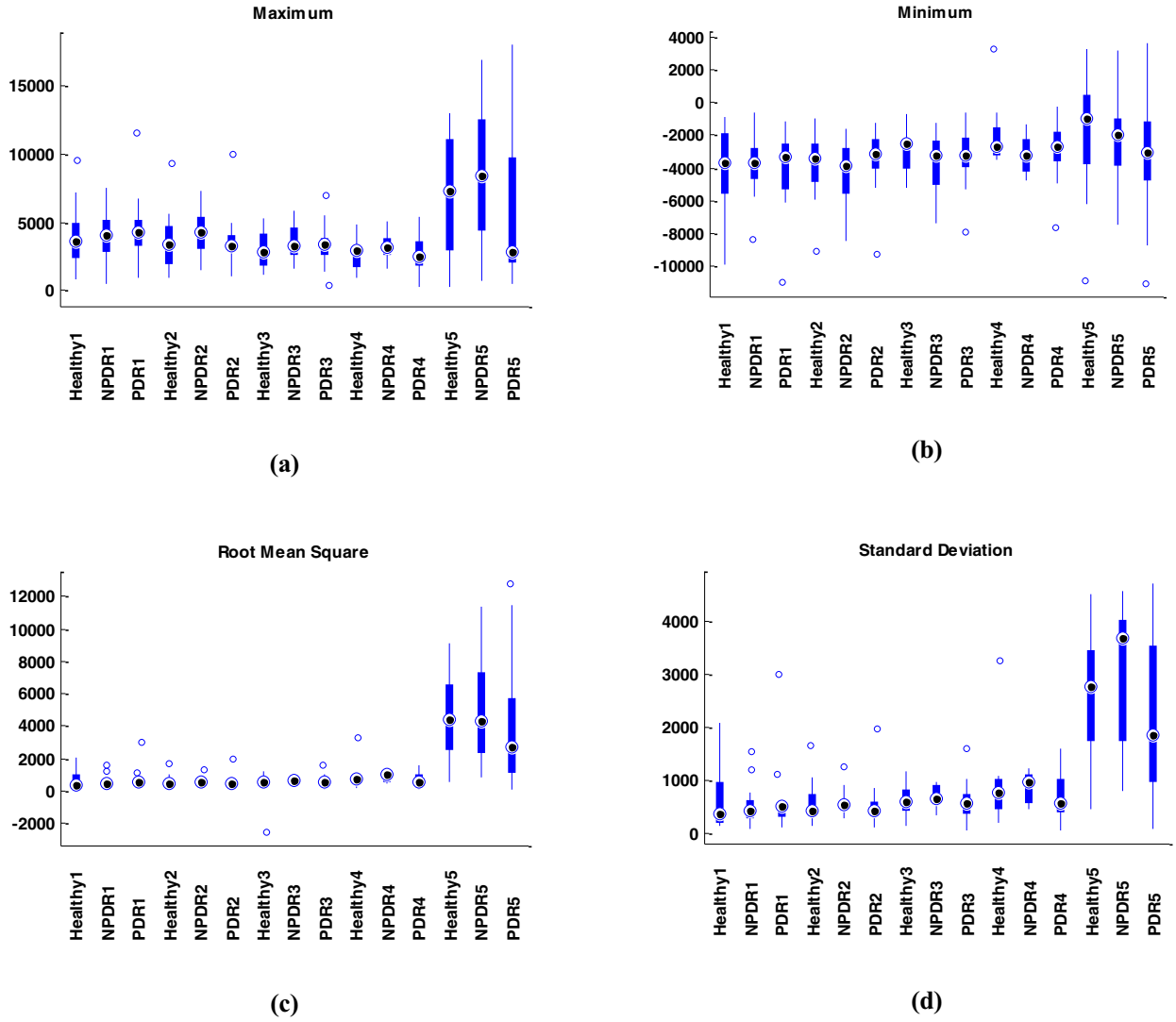

Fig. 7. Statistical features of Right Horizontal DWT coefficients for Healthy, NPDR and PDR VOG Signals (a) maximum, (b) minimum, (c) root mean square and (d) standard deviation. The figure provides range of variation (min-max) and deviations of low-frequency coefficient (A4) and high-frequency coefficients (D1-D4) during wavelet decomposition for right horizontal VOG signal.

Table 1
Statistical performance of DWT-ANNPSO model.

Eye movement	Accuracy (%)	Sensitivity (%)	Specificity (%)
Left horizontal	96.00	93.75	96.97
Right horizontal	94.67	92.16	96.05
Left vertical	92.00	87.99	94.06
Right vertical	90.67	86.03	93.08

Table 2
False discovery rate performance of DWT-ANNPSO model.

Eye movement	Healthy class (%)	NPDR class (%)	PDR class (%)
Left horizontal	5.88	0	0
Right horizontal	5.88	0	5.56
Left vertical	0	5.88	5.88
Right vertical	5.88	6.25	5.88

demonstrate different range of variation (min-max). Meanwhile, A4 coefficient is obtained with higher range of min-max variation and deviation than D1-D4 coefficients for each class (Healthy, NPDR and PDR) in Figs. 6 and 7.

Table 3
Statistical performance of HHT-ANNPSO model for left horizontal eye movement.

Left horizontal features	Accuracy (%)	Sensitivity (%)	Specificity (%)
IMF1	90.67	85.78	92.93
IMF2	92.00	87.99	93.97
IMF3	93.33	89.83	94.95
IMF4	94.67	92.03	95.99
IMF1-2	96.00	94.00	97.03
IMF1-3	97.33	95.96	98.01
IMF1-4	98.67	97.92	98.99

Figs. 8 and 9 represent extracted statistical features (maximum, minimum, root mean square and standard deviation) of left and right horizontal four first IMFs (IMF1-4) calculated by HHT for Healthy, NPDR and PDR VOG signals, where Healthy1, Healthy2, Healthy3 and Healthy4 stands for Healthy VOG signal over IMF1, IMF2, IMF3 and IMF4 respectively.

As seen in Figs. 8 and 9, the deviation of the statistical features for the left horizontal IMF signal is obtained with higher than the right horizontal IMF signals. In additional, the outlier points of the right horizontal IMF signals are more than the left horizontal IMF

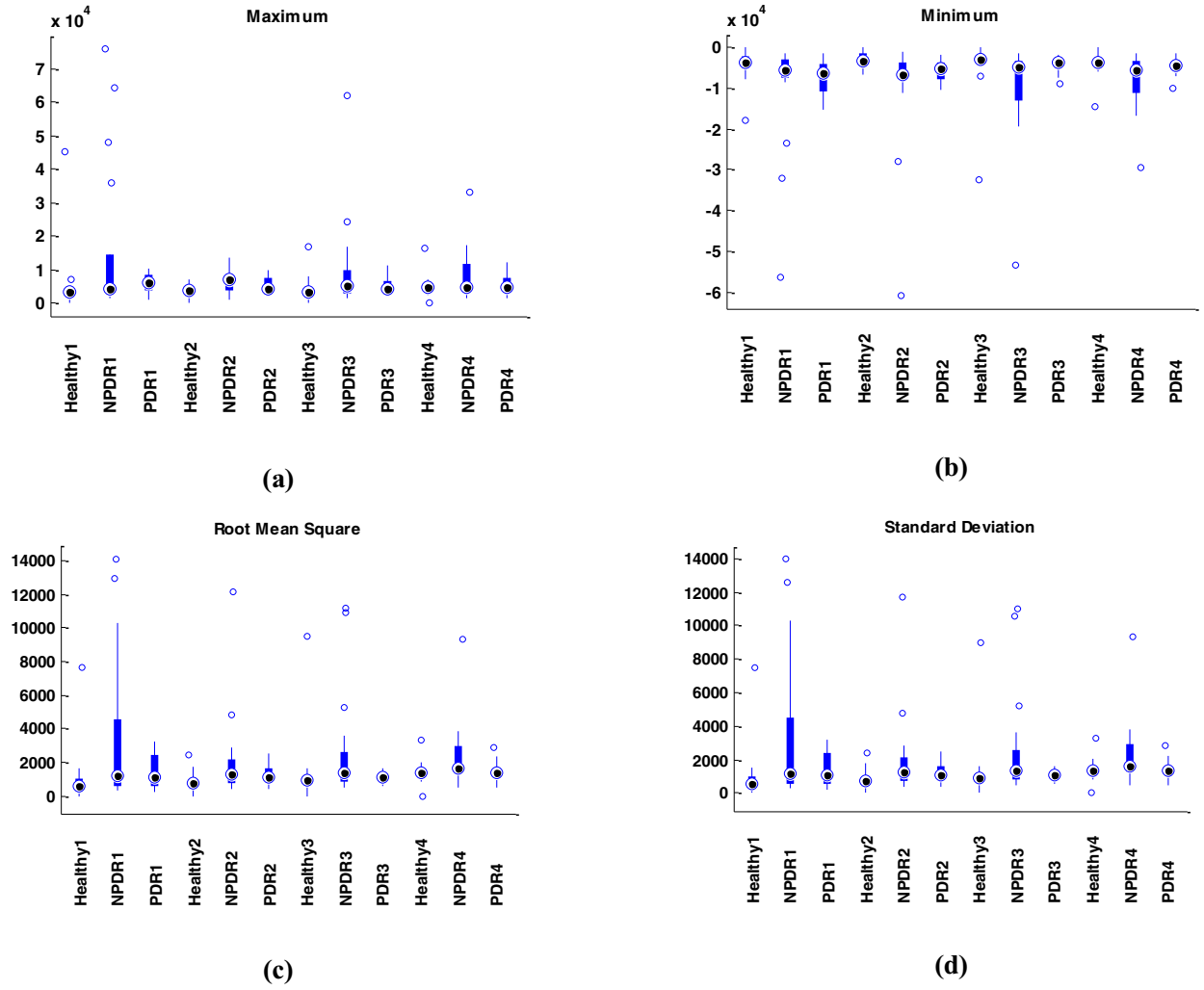

Fig. 8. The range of variation (min-max) and deviation of components (IMF1-4) obtained from 4th level EMD decomposition with left horizontal VOG signal for Healthy, NPDR and PDR, (a) maximum, (b) minimum, (c) root mean square and (d) standard deviation.

Table 4
Statistical performance of HHT-ANNPSO model for right horizontal eye movement.

Right horizontal features	Accuracy (%)	Sensitivity (%)	Specificity (%)
IMF1	89.33	84.19	92.13
IMF2	90.67	85.65	92.90
IMF3	92.00	87.86	93.94
IMF4	93.33	89.70	94.92
IMF1-2	94.67	91.90	95.96
IMF1-3	96.00	93.74	96.94
IMF1-4	97.33	96.08	98.04

Table 5
Statistical performance of HHT-ANNPSO model for left vertical eye movement.

Left vertical features	Accuracy (%)	Sensitivity (%)	Specificity (%)
IMF1	88.00	81.86	90.97
IMF2	89.33	83.69	91.89
IMF3	89.33	83.82	91.92
IMF4	90.67	85.65	92.90
IMF1-2	92.00	87.86	93.94
IMF1-3	93.33	89.57	94.89
IMF1-4	94.67	91.91	96.02

signal. Therefore, the left horizontal IMF features can increase classification performance.

The accuracy analysis (confusion matrix) is realized for each VOG signal to obtain the statistical performance of the models. Statistical performance results of DWT-ANNPSO model are given in Table 1. We show that DWT-ANNPSO model on left horizontal eye movement results in both better accuracy and specificity than right horizontal eye movement. Moreover, DWT-ANNPSO model on left vertical eye movement also performs better in classification with an accuracy of 92.00% and specificity of 94.06% than right vertical eye movement with an accuracy of 90.67% and specificity of 93.08%. It is also seen that DWT-ANNPSO model shows more robust character to classify the disease on horizontal eye movement (average accuracy = 95.33%) than vertical eye movement (average accuracy = 91.33%).

In addition, we apply false discovery rate analysis [33] to show percent of false prediction between three subject classes (Healthy, NPDR and PDR) for the test dataset. False discovery rate performance results of DWT-ANNPSO model are given in Table 2. We show that DWT-ANNPSO model on left horizontal eye movement results in better percentage correct prediction than right horizontal eye movement. Moreover, DWT-ANNPSO model on left vertical eye movement also performs successfully in classification with average false prediction of 3.92% than right vertical eye movement of 6%. It is also seen that DWT-ANNPSO model shows more robust character to classify the disease on horizontal eye movement (aver-

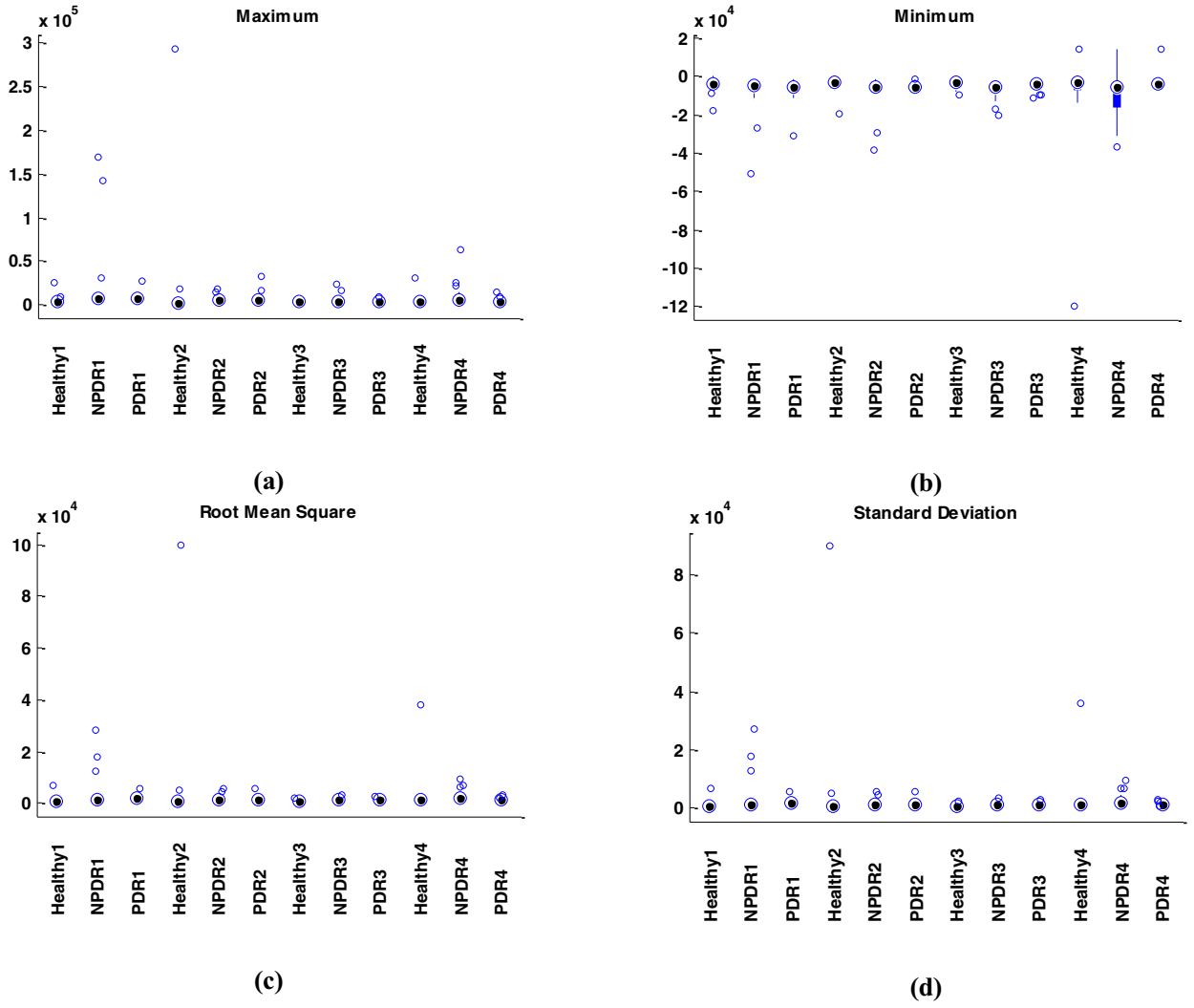

Fig. 9. The ranges of variation (min-max) and deviations of components (IMF1-4) obtained from 4th level EMD decomposition with right horizontal VOG signal for Healthy, NPDR and PDR, **(a)** maximum, **(b)** minimum, **(c)** root mean square and **(d)** standard deviation.

Table 6
Statistical performance of HHT-ANNPSO model for right vertical eye movement.

Right vertical features	Accuracy (%)	Sensitivity (%)	Specificity (%)
IMF1	86.67	80.09	89.95
IMF2	88.00	81.93	90.99
IMF3	89.33	83.76	91.91
IMF4	89.33	83.89	91.94
IMF1-2	90.67	85.72	92.92
IMF1-3	92.00	87.75	93.97
IMF1-4	93.33	89.42	94.74

Table 7
Statistical performance of HHT-ANNPSO model with the IMF1-4.

Eye movement	Accuracy (%)	Sensitivity (%)	Specificity (%)
Left horizontal	98.67	97.92	98.99
Right horizontal	97.33	96.08	98.04
Left vertical	94.67	91.91	96.02
Right vertical	93.33	89.42	94.74

age false prediction = 2.88%) than vertical eye movement (average false prediction = 4.96%).

Then, the performance of seven different HHT-ANNPSO models is analyzed for seven different IMF groups and the results for each eye movement are given in Tables 3–6. As seen in Tables 3–6, IMF1-4 group performs better classification performance on both eye movements than other IMF groups. We show that HHT-ANNPSO model on left horizontal eye movement results in both better accuracy and specificity than right horizontal eye movement for IMF1-4 group. Moreover, HHT-ANNPSO model on left vertical eye movement operates more successfully in classification with an accuracy of 94.67% and specificity of 96.02% than right vertical eye movement with an accuracy of 93.33% and specificity of 94.74% for IMF1-4.

In the light of all the findings, it is seen that multiple IMF Groups (IMF1-2, IMF1-3, IMF1-4) perform robust character than single IMF entries. The best performance between multiple IMF groups is obtained for IMF1–4 group. HHT-ANNPSO model exhibits higher performance on classification of horizontal and vertical eye movements (average accuracy = 98% and 94%, average sensitivity = 97% and 90.66% and average specificity = 98.51% and 95.38% respectively) than DWT-ANNPSO model (average accuracy = 95.33% and 91.33%, average sensitivity = 92.95% and 87.01% and average specificity = 96.51% and 93.57% respectively).

Finally, since the best performance between multiple IMF groups is obtained for IMF1–4 group, we also give the statistical and false discovery rate performance with the IMF1-4 separately in Tables 7 and 8 in order to compare its performance with that

Table 8
False discovery rate performance of HHT-ANNPSO model with the IMF1-4.

Eye movement	Healthy class (%)	NPDR class (%)	PDR class (%)
Left horizontal	5.56	0	0
Right horizontal	0	5.88	0
Left vertical	5.56	0	5.88
Right vertical	0	5.88	5.88

of DWT-ANNPSO model in Tables 1 and 2. The obtained results show that HHT-ANNPSO with the IMF1-4 performs better in classification and has less false discovery rate clearly than the DWT-ANNPSO for each eye movement.

4. Conclusion

This study constitutes a new attempt to introduce the hybrid approach for the diagnosis of diabetic retinopathy by using VOG signals. Two hybrid ANN models based on PSO algorithm are presented. Different four statistical features are extracted from wavelet coefficients by DWT and IMFs by HHT for the training of the models. Therefore, in this study, we first showed the applicability of hybrid DWT-ANNPSO and HHT-ANNPSO models for the diagnosis of diabetic retinopathy by using VOG signals. Our results indicate that HHT-ANNPSO model exhibits better classification performance than DWT-ANNPSO model. We also showed that HHT-ANNPSO with the IMF1-4 provides the best performance.

We have already proposed an ANN model to diagnose diabetic retinopathy by using VOG signals and obtained the classification accuracy of 95.83% [34]. In another study, we suggested a comparative diabetic retinopathy diagnosis study from VOG signals with using ANN model which is trained by DWT and C4.5 algorithm coefficients. We obtained the classification accuracy of 93.75% and 96.87% respectively [35]. In addition, we achieved classification accuracy of 94% using multilayer perceptron neural network (MLP) with diabetic retinopathy by using VOG signals [16]. The obtained results indicate that the HHT-ANNPSO model with the IMF1-4 provides the better performance than the previous ones. Therefore, we may suggest that this model can be used for early diagnosis of diabetic retinopathy.

Since patients with diabetes are under risk of developing diabetic retinopathy, it is essential to classify and stage the severity of diabetic retinopathy earlier [36,37]. We hope that our study will inspire further approaches aimed at the diagnosis of diabetic retinopathy by means of new intelligent decision-making approaches. As a future work, we plan to use different feature extraction methods for pre-processing and research detectability of various eye diseases by using VOG signals. We also plan to use different classification methods such as Support Vector Machine (SVM), Learning Vector Quantization (LVQ) and different Neural Network models to provide the further insight into the classification of diabetic retinopathy.

Acknowledgment

This research is approved by Clinical Research Ethics Committee and supported by Scientific Research Projects Commission of Zonguldak Bülent Ecevit University (Project No: 2015-38701644-01).

References

[1] Kobrin Klein BE. Overview of epidemiologic studies of diabetic retinopathy. Ophthalmic Epidemiol 2007;14(4):179–83.
[2] Jiménez-Báez MV, Márquez-González H, Bárcenas-Contreras R, Morales-Montoya C, Espinosa-García LF. Early diagnosis of diabetic retinopathy in primary care. Colombia Médica 2015;46(1):14–18.
[3] Walter T, Klein JC, Massin P, Erginay A. A contribution of image processing to the diagnosis of diabetic retinopathy-detection of exudates in colour fundus images of the human retina. IEEE Trans Med Imaging 2002;22(10):1236–43.
[4] Vallabha D, Dorairaj R, Namuduri K, Thompson H. Automated detection and classification of vascular abnormalities in diabetic retinopathy. In: Proceedings of 13th IEEE Signals, Systems and Computers; 2004. p. 1625–9.
[5] Pratt H, Coenen F, Broadbent DM, Harding SP, Zheng Y. Convolutional neural networks for diabetic retinopathy. Procedia Comput Sci 2016;90(1):200–5.
[6] Priya R, Aruna P. Diagnosis of diabetic retinopathy using machine learning techniques. ICTACT J Soft Comput 2013;3(4):563–75.
[7] Rajput YM, Manza RR, Patwari MB, Rathod DD, Borde PL, Yannawar PL. Detection of non-proliferative diabetic retinopathy lesions using wavelet and classification using k-means clustering. Int Conf Commun Networks 2015:381–7.
[8] Noronha K, Acharya UR, Nayak KP, Kamath S, Bhandary SV. Decision support system for diabetic retinopathy using discrete wavelet transform. J Eng Med 2012;227(3):251–61.
[9] Rokade PM, Manza RR. Automatic detection of hard exudates in retinal images using haar wavelet transform. Int J Appl Innovat Eng Manag 2015;4(5):402–10.
[10] Solkar S, Das L. A new approach for detection and classification of diabetic retinopathy using pnn and svm classifiers. IOSR J Comput Eng 2017;19(5):62–8.
[11] Lin CS, Lue LW, Yeh MS, Hwang TS, Lee SH. A new image processing method for evaluating the pupillary responses in a HMD-type eye-tracking device. Opt Laser Technol 2003;35(7):505–15.
[12] Clarke AH, Ditterich J, Drüen K, Schönfeld U, Steineke C. Using high frame rate CMOS sensors for three-dimensional eye tracking. Behav Res Methods, Instrum Comput 2002;34(4):549–60.
[13] Chen X, Wenfang L. A pupil location method for Wifi-based video-oculography system. AASRI Procedia 2012;1(1):389–93.
[14] Kim SC, Nam KC, Lee WS, Kim DW. A new method for accurate and fast measurement of 3D eye movements. Med Eng Phys 2006;28(1):82–9.
[15] Hanuška J, Bonnet C, Rusz J, Sieger T, Jech R, Rivaud-Péchoux S, Vidailhet M, Gaymard B, Růžička E. Fast vergence eye movements are disrupted in Parkinson's disease: a video-oculography study. Parkinsonism Rel Disorders 2015;21(7):797–9.
[16] Kaya C, Erkaymaz O, Ayar O, Ozer M. Multi-Layer perceptron and radial basis function neural network models for classification of diabetic retinopathy disease using video-oculography signals. Int J Biomed Biol Eng, World Acad Sci, Eng Technol 2017;11(11):606–11.
[17] Hyvärinen A, Ramkumar P, Parkkonen L, Hari R. Independent component analysis of short-time Fourier transforms for spontaneous EEG/MEG analysis. NeuroImage 2010;49(1):257–71.
[18] Goswami JC, Chan AK. Fundamentals of wavelets. John Wiley & Sons, Inc; 2011. 2nd ed.
[19] Huang NE, Shen Z, Long SR, Wu MC, Shih HH, Zheng Q, Yen NC, Tung CC, Liu HH. The empirical mode decomposition method and the Hilbert spectrum for non-stationary time series analysis. Proc R Soc Lond Ser A 1998:903–95.
[20] Huang NE, Wu Z. An adaptive data analysis method for nonlinear and non-stationary time series: the empirical mode decomposition and Hilbert spectral analysis. In: In Proc. 4th international conference on wavelet and its application; 2007. p. 363–76.
[21] Yan R, Gao RX. Hilbert–Huang transform-based vibration signal analysis for machine health monitoring. IEEE Trans Instrum Meas 2006;55(6):2320–9.
[22] Subaşı A. EEG signal classification using wavelet feature extraction and a mixture of expert model. Expert Syst Appl 2007;32(4):1084–93.
[23] Dixit A, Majumdar S. Comparative analysis of coiflet and daubechies wavelets using global threshold for image denoising. Int J Adv Eng Technol 2013;6(5):2247–52.
[24] Schneck ME, Shupenko L, Adams AJ. The fast oscillation of the EOG in diabetes with and without mild retinopathy. Documenta Ophthalmol 2008;116(3):231–6.
[25] Erkaymaz H, Ozer M, İM Orak. Detection of directional eye movements based on the Electrooculogram signals through an artificial neural network. Chaos Solitons Fractals 2015;56(1):202–8.
[26] Kaya C, Erkaymaz O, Ayar O, Ozer M, dalgacık Ayrık. dönüşümü kullanarak Video-okülografi (VOG) sinyallerinden diyabetik retinopati hastalığının fizyolojik etkilerinin belirlenmesi. Tıp Teknolojileri Ulusal Kongresi 2016:142–5.
[27] Erkaymaz O, Ozer M. Impact of small-world network topology on the conventional artificial neural network for the diagnosis of diabetes. Chaos, Solitons Fractals 2016;83(1):178–85.
[28] Erkaymaz O, Ozer M, Perc M. Performance of small-world feedforward neural networks for the diagnosis of diabetes. Appl Math Comput 2017;311(1):22–8.
[29] Atyabi A, Luerssen MH, Powers DM. PSO-based dimension reduction of EEG recordings: implications for subject transfer in BCI. Neurocomputing 2013;119(1):319–31.
[30] Ahirwal MK, Kumar A, Singh GK. Adaptive filtering of EEG/ERP through noise cancellers using an improved PSO algorithm. Swarm Evolut Comput 2014;14(1):76–91.
[31] Shirvany Y, Edelvik F, Jakobsson S, Hedström A, Persson M. Application of particle swarm optimization in epileptic spike EEG source localization. Appl Soft Comput 2013;13(5):2515–25.
[32] Phinyomark A, Nuidod A, Phukpattaranont P, Limsakul C. Feature extraction and reduction of wavelet transform coefficients for EMG pattern classification. Elektronika ir Elektrotechnika 2012;122(6):27–32.
[33] Benjamini Y, Yekutieli D. The control of the false discovery rate in multiple testing under dependency. Ann Stat 2001:1165–88.
[34] Kaya C, Erkaymaz O, Ayar O, Ozer M. Video-okülografi (VOG) sinyallerinden

diyabetik retinopati hastalığının yapay sinir ağları ile tespiti. 25. IEEE Sinyal İşleme ve İletişim Uygulamaları Kurultayı 2017:1–4.
[35] Kaya C, Erkaymaz O, Ayar O, Ozer M. C4.5 karar ağacı temelli öznitelik seçimi ile Video-okülografi (VOG) sinyallerinden diyabetik retinopati hastalığının sınıflandırılması. Tıp Teknolojileri Ulusal Kongresi 2017:75–8.
[36] Wu L, Fernandez-Loaiza P, Sauma J, Hernandez-Bogantes E, Masis M. Classification of diabetic retinopathy and diabetic macular edema. World J Diab 2013;4(6):290–4.
[37] Shaw JE, Sicree RA, Zimmet PZ. Global estimates of the prevalence of diabetes for 2010 and 2030. Diab Res Clin Pract 2010;87(1):4–14.